

Mass spectrometry-based proteomics to study gastric carcinogenesis: pathophysiological molecular characterization

Nayra Felípez

NavarraBiomed

Sheyla Montori

NavarraBiomed

Alba Valero

NavarraBiomed

Enrique Santamaría

NavarraBiomed

Karina Ausin

NavarraBiomed

Erika Peral

NavarraBiomed

Joan Llach

Fundació de Recerca Clínic Barcelona-Institut d'Investigacions Biomèdiques August Pi i Sunyer

Pedro Delgado

Hospital of Mérida

Pablo Florez-Diez

Hospital Universitario Central de Asturias

Eva Barreiro

Hospital Universitario Central de Asturias

Elena Arruebo

Hospital Universitario Miguel Servet

Raquel Vicente

Hospital Universitario Miguel Servet

M Teresa Soria

Hospital Universitario Miguel Servet

Alain Huerta

Hospital de Galdakao

Silvia Patricia Ortega

Hospital Comarcal de Inca

Henar Núñez

Hospital Universitario Río Hortega

Pilar Díez

Hospital Universitario Río Hortega

Alberto Herreros

Hospital Universitario Puerta de Hierro Majadahonda

Gadea Hontoria

University Hospital of Burgos

Rosa María Saíz

University Hospital of Burgos

Luis Hernández

Hospital Santos Reyes

Carolina Mangas-Sanjuan

Hospital General Universitario de Alicante Doctor Balmis

Oliver Patrón

Hospital Parque de Llevant

Gonzalo Hijos-Mallada

Hospital Clínico Universitario Lozano Blesa

María José Domper-Arnal

Hospital Clínico Universitario Lozano Blesa

Sara Zarraquiños

Hospital Universitario de Ourense

Astrid Irene Díez-Martín

Hospital Universitario de Ourense

Patricia Gonçalves

Clínica ServiDigest

Diego de Frutos

Hospital Universitario Puerta de Hierro Majadahonda

José Santiago

Hospital Universitario Puerta de Hierro Majadahonda

Adelina García

Hospital Universitario Clínico San Cecilio

Alicia Martín-Lagos

Hospital Universitario Clínico San Cecilio

Fermín Estremera-Arévalo

Complejo Hospitalario de Navarra

Marta Gómez Alonso

Compleio Hospitalario de Navarra

Anabella Cuestas

Fundació de Recerca Clínic Barcelona-Institut d'Investigacions Biomèdiques August Pi i Sunyer

Francesc Balaguer

Fundació de Recerca Clínic Barcelona-Institut d'Investigacions Biomèdiques August Pi i Sunyer

Sergi Castellví-Bel

Fundació de Recerca Clínic Barcelona-Institut d'Investigacions Biomèdiques August Pi i Sunyer

Glòria Fernandez-Esparrach

Fundació de Recerca Clínic Barcelona-Institut d'Investigacions Biomèdiques August Pi i Sunyer

Miriam Cuatrecasas

Fundació de Recerca Clínic Barcelona-Institut d'Investigacions Biomèdiques August Pi i Sunyer

Leticia Moreira

Fundació de Recerca Clínic Barcelona-Institut d'Investigacions Biomèdiques August Pi i Sunyer

Joaquín Fernández-Irigoyen

NavarraBiomed

Eduardo Albéniz

edualbeniz@hotmail.com

Complejo Hospitalario de Navarra

EpiGASTRIC EDGAR Consortium

Article

Keywords: gastric cancer, proteomics, premalignant lesions, NF-κB p65, p38MAPK

Posted Date: October 23rd, 2025

DOI: https://doi.org/10.21203/rs.3.rs-7685514/v1

License: © ① This work is licensed under a Creative Commons Attribution 4.0 International License. Read Full License

Additional Declarations: Competing interest reported. Eduardo Albéniz has a consulting agreement with Creo Medical, AGS MedTech, honoraria for lectures, teaching activities or travel grants from Olympus, Boston, Fujifilm, Norgine, Casen Recordati, 3D Matrix. The remaining authors disclose no conflicts.

Abstract

Background

Gastric cancer (GC) remains a major global health challenge, ranking as the fifth most common malignancy. This study employs a proteomic approach to identify stage-specific proteomic signatures at different stages of gastric carcinogenesis, including chronic gastritis (CG), intestinal metaplasia and low-grade dysplasia (IM-LGD) and advanced stages such as early GC (EGC) and GC, to better understand GC pathogenesis.

Methods

The EpiGASTRIC/EDGAR study is a prospective, multicentre, population-based study across Spain. Forty-six patients and seventy-two human gastric tissue samples were employed for proteomic analysis using mass spectrometry: 10 were controls (normal gastric mucosa), 10 CG, 7 IM-LGD, 10 EGC and 9 GC. Samples were collected from lesional (L) and non-lesional (NL) areas in IM-LGD, EGC, and GC. Total and phospho-specific levels of p65 NF-κB and p38MAPK were measured using western blot.

Results

Across the 3.272 quantified proteins, distinct subsets of proteins displayed differential modulation depending on the pathological or non-pathological nature of the tissue. Pathways related to electron transport, oxidative phosphorylation, and mitochondrial import exhibited an inhibitory trend across all cohorts. In contrast, specific pathways such as the degradation of the extracellular matrix and microautophagy signaling were modulated only in the malignancy stages. Western blot revealed coordinated activation of p65 NF-kB and p38 MAPK pathways, particularly in the transition from CG to IM-LGD to EGC. The observation of elevated pp38 levels in IM-LGD-L, unlike pp65, suggests a distinct role for these kinases in areas of cellular transformation.

Conclusions

Distinct activation patterns of NF-κB p65 and p38MAPK were observed, suggesting they are crucial targets in gastric carcinogenesis. Further research is needed to elucidate how their post-translational modifications drive malignant transformation.

Trial registration:

clinicaltrials.gov (NCT05551416; first posted September 22 2022).

Background

Gastric cancer (GC) remains a major global health challenge, ranking as the fifth most common malignancy and as a cause of cancer-related mortality worldwide [2]. This complex and heterogeneous disease is broadly classified based on anatomical location into cardial and non-cardial subtypes [3]. The etiology differs significantly: while lifestyle factors such as obesity and gastroesophageal reflux are strongly implicated in cardial GC, particularly in Western populations [4], *Helicobacter pylori* (*H. pylori*) infection is the predominant risk factor for non-cardial GC, accounting for nearly 90% of cases globally [5].

Histologically, GC is further categorized into two major subtypes: intestinal (IGC) and diffuse (DGC) [6]. DGC is characterized by scattered poorly differentiated cells lacking glandular organization, whereas IGC follows the Correa Cascade, a progressive sequence of pathological changes from chronic gastritis to gastric adenocarcinoma [7, 8]. Despite the well-established association between *H. pylori* and GC, only a small fraction of infected individuals develop GC, highlighting the role of additional genetic, environmental, and host-related factors in its pathogenesis [5].

Recent advances in molecular profiling have unveiled a diverse landscape of genetic and epigenetic alterations in GC, identifying distinct subtypes, including Epstein-Barr virus-positive, microsatellite instability, chromosomal instability, and genomic stable tumors [9]. Proteomic studies have further contributed to our understanding by identifying protein signatures associated with disease progression and early detection. In particular, profiling of precancerous lesions has provided insights into molecular alterations driving the transition from early gastric cancer (EGC) to advanced GC [10, 11]. Additionally, multilevel analyses revealed subtype-specific differences in signaling pathways, protein expression, and clinical behavior [12].

This study employs a proteomic approach to characterize benign and precancerous stages such as chronic gastritis (CG), intestinal metaplasia and low-grade dysplasia (IM-LGD), and neoplastic stages such as EGC and GC. Specifically, this research seeks to (i) identify stage-specific proteomic signatures by determining differentially expressed proteins (DEPs) across lesional (L) and non-lesional (NL) tissues, (ii) analyzed disrupted biological processes to understand their role in gastric carcinogenesis; (iii) characterize shared and distinct protein deregulation patterns between early and advanced stages; and (iv) develop a systems biology framework to map protein interactions and identify key molecular regulators driving gastric carcinogenesis. These insights may contribute to a deeper understanding of GC pathogenesis and support the development of effective strategies for prevention, early detection and treatment.

Methods

Design and study population

The EpiGASTRIC/EDGAR study is a prospective, multicentre, population-based study with a broad geographic representation of the Spanish population affected by GC and premalignant gastric lesions (PGLs). It includes distinct yet interrelated cohorts: symptomatic patients undergoing diagnostic gastroscopy without known gastric pathology or a family history of GC (EDGAR 1); patients with PGLs and early gastric neoplasms treated via endoscopic resection (EDGAR 2); and patients diagnosed with GC (EpiGASTRIC). The inclusion period for this study was from April 2022 to May 2024. It was also registered at clinicaltrials.gov (NCT05551416; first posted September 22 2022).

Participants were recruited from 28 hospitals across Spain equipped with advanced gastroenterology and endoscopy units. The study was conducted in compliance with the Declaration of Helsinki (Fortaleza, Brazil, October 2013 version). It was carried out in accordance with the protocol and relevant legal requirements, based on Law 14/2007 of July 3, on biomedical research. The study protocol was reviewed and approved by the Research Ethics Committees at each participating center. Informed consent was obtained from all participants before endoscopic procedures and they could revoke their consent at any time during the study.

Data and sample collection

Clinical and demographic data were collected on the REDCap-AEG online platform, which researchers from each center can access through an identification code under the current Spanish Organic Law on Data Protection. The data collected included personal and clinical information such as age, sex, weight, comorbidities, lifestyle factors, medical history, and detailed endoscopic and histological data.

All participants included in the study underwent upper gastrointestinal endoscopy. Endoscopic evaluations followed standard sedation/anesthesia protocols, and samples collected during procedures were immediately processed and stored. Stomach tissue samples were immediately frozen at -80°C.

Samples for this specific study were collected from 46 patients and 72 frozen gastric tissue samples were used for proteomic analysis. In premalignant and malignant cohorts, both L and NL samples were obtained from each patient. L tissue was defined as gastric mucosa with histologically confirmed premalignant (IM-LGD) or malignant changes (EGC and GC), and was collected in a targeted manner from the area identified during endoscopy. NL tissue was defined as normal mucosa without abnormalities, obtained randomly from the antrum and body within the same patient.

Diagnoses were established based on current clinical guidelines and patients were categorized according to histopathological results obtained through out upper gastrointestinal endoscopies.

Materials

Antibodies for pp38 MAPK (Thr180/Tyr182) (#9211), p38 MAPK (#9212), pNF-κB p65 (#3033) and NF-κB p65 (#8242). Electrophoresis reagents were purchased from Biorad (Hercules, CA, USA), and trypsin

was purchased from Promega (Madison, WI, USA). Antibodies and dilutions used in this study are shown in Additional file 1: Table S1.

Gastric tissue preparation for proteomic analysis

Human gastric tissue samples were homogenized in a lysis buffer (8 M urea, 50 mM dithiothreitol (DTT)). Lysates were centrifuged at 100,000 x g (1 h, 15°C), and the resulting supernatant was quantified with the Bradford assay kit (BioRad, Barcelona, Spain). Proteins were reduced with DTT (final concentration of 20 mM; room temperature, 30 min), alkylated with iodoacetamide (final concentration of 30 mM; room temperature, 30 min in the dark), diluted to 0.9 M with ABC and digested with trypsin (Promega, Madison, WI, USA; 1:20 w/w enzyme protein ratio, 18 h, and 37°C). Protein digestion was interrupted by acidification (pH < 6, acetic acid), and the resulting peptides were cleaned up using Pierce™ Peptide Desalting Spin Columns (ThermoFisher Sci., Waltham, MA, USA).

Data independent acquisition (DIA)-mass spectrometry

Dried-down peptide samples were reconstituted with 2% ACN-0.1% FA (Acetonitrile-Formic acid), spiked with internal retention time peptide standards (iRT, Biognosys), and quantified by NanoDropTM spectrophometer (ThermoFisher Sci.) before LC-MS/MS analysis using an EVOSEP ONE chromatography system coupled to an Exploris 480 mass spectrometer (Thermo Fisher Sci.). Peptides were resolved using the C18 Performance column (75µm x 15cm, 1.9 µm particles; Evosep) with a predefined Xcalibur Whisper100 20 SPD (58min, IonOpticks Aurora Elite, EV1112) method. Peptides were ionized using a 1.6 kV spray voltage at a capillary temperature of 275°C. Sample data were acquired in data-independent acquisition (DIA) mode with full MS scans (scan range: 400 to 900 m/z; resolution: 60,000; maximum injection time: 22 ms; normalized AGC target: 300%) and 24 periodical MS/MS segments applying 20 Th isolation windows (0.5 Th overlap: Resolution: 15000; maximum injection time: 22 ms; normalized AGC target: 100%). Peptides were fragmented using a normalized HCD collision energy of 30%.

Bioinformatics and statistical analysis

Mass spectrometry data files were analyzed using Spectronaut (Biognosys) by direct DIA analysis (dDIA). Using standard settings, MS/MS spectra were searched against the Uniprot proteome reference from the human database. The enzyme was set to trypsin in a specific mode, Carbamidomethyl (C) was set as a fixed modification, and oxidation (M), acetyl (protein N-term), deamidation (N), and Gln->pyro-Glu as variable modifications. Identifications were filtered by a 1% FDR.

The obtained quantitative data for total protein were exported to Perseus software (version 1.6.15.0) [13] for statistical analysis and data visualization. Unpaired Student's t-test was used for direct comparisons. Statistical significance was set at a p-value lower than 0.05 in all cases. DEPs were deemed significant

when their absolute fold change was below 0.77 (downregulated proteins) and above 1.3 (up-regulated proteins) on a linear scale.

Enrichment analysis was assessed using Metascape [14], based on Reactome Database and applying default settings (min. overlap: 3, min. enrichment: |1.5|, P < 0.05). Protein interactomes and activation ranking were analyzed using QIAGEN's Ingenuity Pathway Analysis (IPA; QIAGEN Redwood City) [15].

To compare protein expression, we performed statistical analyses using the *stats* (v4.4.2) and *car* (v3.1-3) packages in RStudio (v4.4.2). We conducted group comparisons using Student's t-test (paired or unpaired, with or without Welch correction) or the Wilcoxon rank-sum test.

For data visualization, we used ggplot2 (v3.5.1) to create jittered boxplots and barplots with error bars and significance annotations. We considered a value of p < 0.05 statistically significant (*), p < 0.01 very significant (**), and p < 0.001 highly significant (***).

Western-blotting

Equal amounts of gastric tissue protein derived from human samples (12 μg) were resolved in 4–15% stain-free SDS–PAGE gels (BioRad) and electrophoretically transferred onto nitrocellulose membranes using a Trans-blot Turbo transfer system (up to 25 V, 7 min) (BioRad). Per manufacturer instructions, membranes were incubated overnight at 4°C with primary antibodies diluted to 1:1000 in 5% BSA. Finally, membranes were incubated with the appropriate horseradish peroxidase-conjugated secondary antibody (1:5000), and immunoreactive proteins were visualized by enhanced chemiluminescence (Perkin Elmer) and detected by a Chemidoc MP Imaging System (BioRad). Equal loading of the gels was assessed using stain-free imaging technology. After densitometric analyses (Image Lab Software Version 5.2; Bio-Rad), optical density values were expressed as arbitrary units and normalized to total protein levels in each gel lane.

Results

Proteomic landscape across normal, preneoplastic and neoplastic gastric tissue

We employed a DIA-MS-based approach to characterize the proteomic landscape of the stomach. A total of 46 patients were included: 10 controls, 10 with CG, 7 with IM-LGD, 10 with EGC and 9 with GC. Among them, 27 (58.7%) were women and 19 (41.3%) were men, with a mean age of 64.4 years (SDs 15.2). The descriptive data of the participants are shown in Table 1. Biopsies from patients with IM-LGD, EGC and GC were taken from L and NL areas (Additional file 1: Table S1).

Table 1

Baseline characteristics of the participants according to the cohort. Categorical variables are described by numbers (percentages) and continuous variables by means (± SDs). * CG = chronic gastritis, IM-LGD = intestinal metaplasia-low grade dysplasia, EGC = early gastric cancer, and GC = gastric cancer, *H. pylori* = Helicobacter pylori.

Characteristics		Control (n =	CG	IM-LGD (n	EGC (n =	GC
		10)	(n = 10)	= 7)	10) `	(n = 9)
Age, years, mean (SD)		58.1 ± 9.0	54.8 ± 14.9	70 ± 10.1	76.6 ± 12.1	64.3 ± 18.4
Sex, n (%)						
	Women	5 (50.0)	5 (50.0)	3 (42.9)	8 (80.0)	5 (55.6)
	Men	5 (50.0)	5 (50.0)	4 (57.1)	2 (20.0)	4 (44.4)
Smoking, n (%)						
	Former	6 (60.0)	5 (50.0)	0 (0.0)	2 (20.0)	3 (33.3)
	Never	3 (30.0)	4 (40.0)	5 (71.4)	7 (70.0)	4 (44.4)
	Current	1 (10.0)	1 (10.0)	2 (28.6)	1 (10.0)	2 (22.2)
Alcohol intake, n (%)						
	Current	9 (90.0)	9 (90.0)	4 (57.1)	5 (50.0)	5 (55.6)
	Never	1 (10.0)	1 (10.0)	3 (42.9)	5 (50.0)	4 (44.4)
Current <i>H. pylori</i> infection						
	Yes	-	7 (70.0)	1 (13.3)	1 (10.0)	-
	No	10 (100.0)	3 (30.0)	6 (86.7)	6 (60.0)	-
	N/C	-	-	-	3 (30.0)	9 (100.0)

Across the 3.272 quantified proteins from all experimental groups, we identified distinct subsets of proteins displaying differential modulation depending on the pathological or non-pathological nature of the tissue (Fig. 1A-F and Additional file 2: Figure S1). These modulations varied according to disease stage (Fig. 1C, 1F), revealing stage-specific proteomic signatures as the disease progressed. Moreover, we found that specific components of the differential stomach proteome were consistently altered across different malignancy stages (Fig. 1G), suggesting shared molecular mechanisms underlying gastric carcinogenesis.

Our analysis identified 728, 1.019, 1.220, and 338 DEPs in CG, IM-LGD-L, EGC-L, and GC-L samples (Fig. 2). Despite a relatively balanced distribution of upregulated and downregulated proteins across these stages (Fig. 2A), elevated protein levels were particularly prominent during the IM-LGD-L and EGC-L

stages, likely reflecting heightened cellular activity related to inflammation, tissue repair, and immune responses—processes standard in precancerous and early stages [16].

Despite these general trends, 136 DEPs were consistently modulated across all stages and 54 DEPs were uniquely associated with malignant transformation (Fig. 2B). (Additional file 3: Table S2). In contrast, NL tissue from IM-LGD, EGC, and GC exhibited 334, 120, and 1.078 DEPs, respectively (Fig. 2C). Among these, 40 DEPs were common across the three stages (Fig. 2D).

Only four DEPs were shared between L and NL tissues (Additional file 3: Table S2 and Additional file 4: Figure S2). These were related to cell adhesion (MAGI1), innate immunity (NLRX), lipid metabolism (CHKB), and apoptosis regulation (TIGAR). Neutrophil degranulation was the only shared signaling pathway between common L and NL tissue proteins (Additional file 4: Figure S2).

Figure 2. Differentially expressed proteins in the stomach across CG, IM-LGD, EGC, and GC. **A**. Differential gastric proteome distribution across L stages. **B**. Venn diagram of standard and unique differential protein between lesional stages. **C**. Differential stomach proteome distribution across non-lesional stages. **D**. Venn diagram of standard and unique differential protein between non-lesional stages. (CG = chronic gastritis, IM-LGD = intestinal metaplasia-low grade dysplasia, EGC = early gastric cancer, and GC = gastric cancer, NL = non-lesional, L = lesional). Barplots were made using Biorender.com and diagrams with online tool [17].

Commonalities and differences across tissue types

To uncover common and distinct biological processes associated with gastric carcinogenesis, stage-dependent proteomic datasets from NL and L gastric tissues were subjected to functional enrichment analysis. As shown in Figs. 3A, 3B, functional similarities were observed between L and NL tissues across disease stages. Vesicle-mediated transport, extracellular matrix organization, trans-Golgi network vesicle budding, and neutrophil degranulation pathways were commonly enriched in L and NL gastric tissue (Fig. 3A, 3B). However, distinct pathways, such as aflatoxin activation and detoxification, expressed lesion-specific disruption across IM-LGD, EGC, and GC (Fig. 3A).

Pathway enrichment and shared DEPs between EGC-L and GC-NL tissues

The analysis revealed several intriguing comparisons across different tissues (Additional file 5: Table S3). Notably, we observed significant enrichment of specific pathways between EGC-L and GC-NL tissues, which appeared similar based on quantification results. These two cohorts exhibited the highest number of DEPs, with 796 DEPs common between them. Key enriched pathways included rRNA processing, lysine catabolism, and phase II: conjugation of compounds (Figs. 3A, B). In rRNA processing, 25 common proteins were identified (Additional file 6: Figure S3), primarily upregulated (e.g., NOB1, BYSL, RPS15A, EBNA1BP2, GNL3), with only two downregulated (RPL22, HSD17B10). Lysine catabolism showed downregulation of all three common proteins (DLST, GCDH, and DHTKD1) (Additional file 6:

Figure S3). Phase II: conjugation of compounds also displayed predominantly inhibited proteins, except for PAPSS2 and TRMT112 (Additional file 6: Figure S3).

Enriched pathways in premalignant and advanced stages of gastric carcinogenesis

Regarding gastric carcinogenesis, aflatoxin activation and detoxification were uniquely enriched in malignant stages (Fig. 3A), involving MGST1, MGST3, and AKR7A3 (Additional file 7: Figure S4). AKR7A3 is associated with AFB1 detoxification, protecting against its carcinogenic effects [18]. Formation of fibrin clot (clotting cascade) and antimicrobial peptides were consistently present across both tissue types (Figs. 3A, B). PRTN3 was the sole common protein, upregulated across almost all tissues (not in CG), with higher significance in L and GC-NL tissues (Additional file 7: Figure S4).

Protein expression changes were also observed during the transition from early to advanced cancer. Pathways such as vpr-mediated induction of apoptosis, signaling by high-kinase activity BRAF, hyaluronan uptake and degradation, and mutants' regulation of IGF transport, were enriched in IM-LGD-L, EGC-L, and GC-NL, but diminished in advanced L tumors (Figs. 3A, B). This included the downregulation of SLC25A4, SLC25A5, and SLC25A6 in apoptosis induction, and upregulation of CSK, FGA, FGB, CD44, GUSB, APOB, APOE, C3, CP, FGA, FUCA2, ITIH2, and PLG in the other three pathways (Additional file 8: Figure S5).

Consistently dysregulated pathways: aerobic respiration and neutrophil degranulation

Focusing on the most significantly altered pathways (with higher z-scores), we found that aerobic respiration, respiratory electron transport, and neutrophil degranulation were consistently dysregulated throughout disease progression (Figs. 3A, B). Within respiratory electron transport, a core set of proteins, including UQCRFS1, VDAC1, COX4I1, NDUFS3, NDUFB3, NNT, NDUFB8, NDUFA9, COX6C, NDUFS2 and UQCRQ, exhibited consistent inhibition across tissue types, from CG to GC-L, including its adjacent tissues (except EGC-NL) (Additional file 9: Figure S6). Further analysis revealed specific protein expression changes: MDH1 was downregulated from IM-LGD-L to GC-L, including its adjacent tissue (Fig. 3C), PDP1 inhibition was exclusively detected in precancerous or early stages (Fig. 3D), and NDUFB6 was inhibited only in the three L tissues (Fig. 3E). Similarly, neutrophil degranulation displayed a common set of upregulated proteins, including CTSZ, ITGB2, GYG1, PRTN3, and GGH (Additional file 10: Figure S7). This pathway showed altered expression across all disease stages, regardless of tissue type (Figs. 3A, B). Specifically CAMP, S100A11, ANPEP, STOM, MMP9, PGLYRP1, LTF, MVP, SERPINB1, HSPA8, HEXB and CCT8 were upregulated, whereas COTL1, CKAP4 and MAGT1 were downregulated compared to healthy donors (Figs. 3G-J and Additional file 11: Figure S8). To highlight the dynamics of the alterations, we focused on key proteins demonstrating notable patterns. STOM was upregulated in EGC-L, GC-L, and GC-NL, and ANPEP in EGC-L, EGC-NL, GC-L, and GC-NL (Figs. 3H, I). Discontinuous expression changes were observed in CAMP upregulation in IM-LGD-L, GC-L, and GC-NL (Fig. 3F), and

COTL1 downregulation in IM-LGD-L and EGC-L (Figs. 3J). Finally, S100A11 was consistently upregulated across all three malignancy stages (Fig. 3G).

Pathway-specific alterations during gastric carcinogenesis

We constructed protein-scale interaction networks to explore the cooperative interactions among DEPs, focusing on proteins deregulated across various GC stages (Fig. 4). Using IPA software, we developed protein interactomes for each stage (pathological and non-pathological). This integrative network-based approach allowed us to uncover deregulated proteins' biological functions and molecular contexts in each stage and create a framework to map interactions between deregulated proteins as the GC cascade progresses. Functional protein interaction networks revealed distinct deregulation patterns across the stages of gastric pathology, including CG, IM-LGD, EGC, and GC. Regardless of the tissue state (benign vs. malignant), there was a certain level of protein deregulation, with some proteins being upregulated (red) and others downregulated (green) (Figs. 4A-D). Even in premalignant stages, such as CG (Fig. 4A), kinases like Akt appear as central nodes in the signaling pathway. As the lesion worsens, the interactions become more complex, with dense connections between deregulated proteins (Figs. 4B-D). The complexity of the network reflects widespread dysfunction in molecular pathways, characteristic of advanced cancer. Signaling hubs such as ERK, AMPK, and MAPK were especially prominent in GC-L (Fig. 4D), underscoring their critical role in regulating cancer progression. Subsequent experiments were performed to monitor the activation state of some of these kinases across GC staging. Given their central role in inflammatory and tumorigenic pathways, we focused on NF-kB and p38MAPK. Western blot analyses were conducted to evaluated total and residue-specific phosphorylation of pNF-kB p65/NFκB p65 and pp38MAPK/p38MAPK (Figs. 4E-G).

As shown in Figs. 4E and 4F, CG tissues exhibited a significant increase in total p65 and pp65, indicating heightened NF-kB activity within this inflammatory environment. Delving into IM-LGD tissues, our analysis unveiled a significant upswing in total p65 across L and NL areas, while pp65 was higer in NL tissue, aligning with the likely presence of inflammation, possibly gastritis(Fig. 4F). Moving to EGC, we found a significant increase in total p65 and pp65, indicating a progressive increase in NF-kB activation during gastric carcinogenesis(Figs. 4E, F). This pattern remained consistent when comparing EGC to the control and more advanced cancer groups, IGC and DGC (Figs. 4E, F). A discernible shift in the p65 NF-kB activation pattern emerged in IGC and DGC. Both subtypes displayed a similar trend of pp65 downregulation (Fig. 4E). However, total p65 levels persisted significantly higher in DGC across L and NL tissue (Fig. 4F).

Additionally, the data showed in CG a noticeable, though not statistically significant, increase in pp38 and p38 MAPK levels compared to control (Figs. 4G, H), suggesting a possible compensatory role for p38 MAPK in gastritis' inflammatory response alongside pp65 NF-kB. In IM-LGD tissues, total p38 is elevated in L and NL tissues (Fig. 4G), but unlike pp65 NF-kB, pp38 MAPK levels were higher in L areas (Fig. 4H). In EGC, we observed differentials in total and phosphorylated p38 MAPK levels. While total p38 MAPK levels were similar between NL and L tissues (Fig. 4H), pp38 MAPK was predominantly higher in L tissue when compared with the control group and advanced cancer stages (Fig. 4G). This contrasts with the

trend observed for p65 NF-kB, where total p65 levels were higher in L tissue, while pp65 was slightly higher in NL tissue (though no statistical significance within the same cohort was found). This could suggest a shift in the regulatory mechanisms of p38 MAPK activation in EGC, where phosphorylation and, thus, activation of p38 is favored in the tumor microenvironment despite similar overall protein levels in surrounding areas. EGC demonstrates a significant pp38 MAPK increase, mirroring the considerable rise in both p65 and pp65 observed in this stage, strengthening the argument for coordinated inflammatory pathway activation in gastric carcinogenesis. In advanced stages, IGC and DGC, the pattern diverges. While pp38 MAPK shows a trend towards reduction, particularly in IGC (Fig. 4G), p38 remains elevated, specifically in DGC (Fig. 4H). This parallels the complex shift in p65, where pp65 was downregulated, but total p65 remained high in DGC.

Activation and inhibition patterns of upstream regulators and signaling pathways across lesional and non-lesional gastric tissue.

Analysis of upstream regulators were performed using IPA. The analysis revealed potential changes in the activation state of signaling pathways, upstream regulators, and biological functions based on the expression patterns of DEPs across stages (Fig. 5). According to the profiles of DEPs, pathways related to electron transport, oxidative phosphorylation, and mitochondrial import exhibited an inhibitory trend across all cohorts (Fig. 5A). In contrast, specific pathways such as the degradation of the extracellular matrix and microautophagy signaling were modulated only in the malignancy stages and in GC-NL (Fig. 5A). Additionally, biological functions such as granulocyte response and oxygen consumption tended to be activated in a stage-modulated manner (Fig. 5B). The analysis also highlighted that the differential gastric proteome identified signaling molecules that were either activated or inhibited during gastric carcinogenesis (Fig. 5C-F), particularly in the IM-LGD-L, EGC-L, and GC-NL cohorts (Fig. 5D, E) or specifically modulated in EGC-L, GC-L, and GC-NL (Fig. 5F).

Discussion

Proteins are well-established players in carcinogenesis. In this study, we identified several biological processes and signaling pathways frequently disrupted by dysregulated proteins during gastric carcinogenesis. Our results confirmed that NF-kB p65 and p38MAPK are crucial targets in the dysregulation of pathways involved in disease progression.

The capability of our analysis to identify several significant upstream regulators associated with GC suggests that our approach effectively captures the signaling dysregulation induced by protein alterations in GC. For example, among the eleven primary upstream regulators linked to advanced malignancy stages, each regulates at least one of the proteins selected for validation (Fig. 5C-F). Supporting this, previous studies have experimentally validated the roles of CREB1 and IL-6 in modulating the MAPK and NF-kB signaling pathways [20, 21]. Several dysregulated proteins controlled by these upstream regulators, such as MMP9, have been linked to cancer progression [22]. However, the direct impacts of all dysregulated proteins in GC have yet to be fully established.

One of the significant findings of the present study is the involvement of NF-κB p65 in the pathogenesis of GC, with its deregulation partially linked to phosphorylation at S536, particularly during early rather than advanced cancer. NF-κB proteins are crucial in enhancing cell growth, inhibiting apoptosis, and promoting invasion and metastasis [23]. Significantly, NF-κB contributes to tumor initiation by suppressing immune surveillance from innate and adaptive immune cells, allowing tumor cells to evade immune detection during early tumorigenesis [24]. This dual function positions NF-κB as a critical mediator in the tumor microenvironment, suggesting that targeting NF-κB signaling pathways may enhance therapeutic strategies to inhibit tumor progression and improve anti-tumour immunity. The p65 subunit, also known as RelA, resides in the cytoplasm as part of an inactive heterodimer complex (p65/p50) [25]. Its activation is triggered by proinflammatory cytokines and in response to microbial and viral infections that activate the tripartite IKK complex [26]. This activation results in the phosphorylation and subsequent degradation of IκB proteins. It releases the NF-κB dimers to translocate to the nucleus and activating gene transcription, regulating processes like inflammation [25, 26].

Hyperactivation of NF-κB during early cancer progression is well documented [27, 28]. However, little is known about p65 alterations in cancer development. Our findings suggest that p65 is dynamically regulated during different GC stages, with post-translational modifications potentially influencing these shifts. Phosphorylation is the most studied mechanism of p65 regulation, with eleven phospho-sites identified to date [29, 30]. Among these, S536 is found in the C-terminal transactivation domain, which controls transcriptional activation and gene expression [29]. Studies have reported an upregulation of p65 phosphorylation at S536 in various cancers. For example, researchers in a Swedish cohort analyzed phospho-S536-p65 in 203 primary colon tumors, 156 normal mucosa samples (82% matched with primary tumors), and 18 lymph node metastases [31]. The results showed higher levels of p65 phosphorylation in primary tumors compared to normal tissue [31]. Additionally, recently, it was found that in hepatocellular carcinoma, p65 phosphorylation mediated by ARRB1 and in response to inflammation was also responsible for tumor progression and proliferation [32]. Nevertheless, the effects of p65 phosphorylation remain controversial. For instance, Pradère et al. demonstrated that phosphorylation at this specific site serves as a negative regulator, inhibiting the transactivation potential of p65 [33]. They found that phosphorylation at S536 disrupts the interaction of p65 with essential coactivators required for the transcription of pro-inflammatory genes, thereby attenuating NFκB-mediated inflammatory responses [33]. Aoki et al. shared a similar approach to Pradère's [34]. However, they dive deeper into how this phosphorylation specifically downregulates inflammatory responses, linking more directly to changes in inflammatory cytokine production [34].

These findings suggest a complex role for p65 phosphorylation at S536. On the one hand, it may enhance pro-inflammatory gene transcription during early tumorigenesis, a hallmark of cancer development. On the other hand, it could act as a regulatory mechanism moderating inflammatory responses in the initial stages, a control that may diminish later. Furthermore, our study raises questions regarding the relationship between p65 phosphorylation and the expression of specific proteins such as MMP9. The overexpression of MMP9 observed in the heatmap (Fig. 5D-F) of EGC-L and GC-L may occur

independently of the phosphorylation of p65 itself, leaving it to be determined what effect this phosphorylation has or ceases to have on the transcription of specific genes.

Given the established contribution of chronic inflammation to tumorigenesis [35], our findings reinforce the role of p38 mitogen-activated protein kinase (MAPK) signaling in the multistep progression of GC. The MAPK pathway responds to external stimuli, including oxidative stress, inflammatory cytokines, ultraviolet radiation, and hypoxia [36]. Among its constituents, the p38 family – particularly the α and $\mathbb N$ isoforms – has been implicated as regulators in digestive tract malignancies [37]. For example, Yin et al. demonstrated that p38 $\mathbb N$ is essential for initiating colon tumors under inflammatory conditions, functioning through pathways that include cytokine release and Wnt/ β -catenin activation [38]. However, the role of p38 MAPK as an oncogene or tumor suppressor remains unclear. Previous literature has emphasized the dualistic role of p38 MAPK, especially p38 α , where its activation may suppress tumor initiation but become necessary for tumor cell survival and proliferation in established colon cancers [39].

Our current findings underscore a dynamic and stage-dependent role of p38 MAPK activation in gastric carcinogenesis, providing novel insights into the differential regulation of this signaling axis across various histopathological stages. Western blot analysis revealed an increase in both total and phosphorylated p38 MAPK in CG, IM-LGD, and EGC tissues, particularly in L areas. These findings are consistent with previous studies indicating that p38 MAPK modulates inflammatory responses and contributes to tissue remodeling during early stages of neoplastic transformation [40, 41]. In fact, Hardwick et al. demonstrated that p38 MAPK signaling pathway is highly active in stromal immune cells of colonic adenomas, suggesting that stromal inflammation may converge with epithelial responses to facilitate tumor initiation [42].

In advanced stages of GC, the p38 MAPK signaling pathway exhibited divergent patterns between IGC and DGC. These findings might explain kinase/phosphatase activity alterations or engagement in non-canonical pathways. The observed reduction in IGC p38 MAPK contrasts with studies in other cancers, such as breast cancer. For instance, HER2 overexpression has been shown to promote early dissemination by inhibiting the p38 pathway through downregulation of MAP3K4, an upstream activator of p38 MAPK [43]. This suppression leads to decreased p38 activation, facilitating cancer cell migration and invasion [43]. Similarly, MacNeil et al. identified MKK3 as a tumor suppressor with reduced copy number leading to impaired p38 activation [44].

In contrast, the sustained expression of p38 MAPK in DGC, despite reduced pp38, suggests alternative roles. Elevated levels might be associated with non-canonical activity. Besides the canonical activation pathway, in which MAP2K-catalysed phosphorylation of Thr180 and Tyr182 is required for active kinase activity, there are also two non-canonical pathways [45]. One involves autophosphorylation of p38 α upon binding with transforming growth factor- β -activated protein kinase 1-binding protein 1 (TAB1) [45, 46]. Another alternative activation mechanism, specific to T cells, is mediated by T cell receptor (TCR)-

proximal tyrosine kinases, specifically ZAP70. Upon TCR stimulation, p38α is activated through phosphorylation at Tyr323, leading to subsequent autophosphorylation at Thr180 and Tyr182 [45, 47].

Conclusion

This study offers essential insights into the molecular alterations associated with gastric carcinogenesis, highlighting the roles of NF-κB p65 and p38 MAPK signaling. Across over 3.000 proteins quantified, distinct subsets of proteins displayed differential modulation depending on the pathological or non-pathological nature of the tissue. Pathways related to electron transport, oxidative phosphorylation, and mitochondrial import exhibited an inhibitory trend across all cohorts. Our findings also suggest that p65 phosphorylation at S536 may either enhance pro-inflammatory gene transcription during early tumorigenesis or act as a regulatory mechanism moderating inflammatory responses. Complementarily, p38 MAPK exhibited a dynamic, stage-dependent role, with divergent patterns observed between IGC and DGC. By analyzing paired L and NL regions, we reduced inter-patient variability and identified potential therapeutic targets, including post-translational modifications of p65 and p38. However, a more extensive number of samples would be essential to validate these findings. Moreover, this study's list of DEPs may be subject to variability introduced by cohort-specific factors and confounding variables. In particular, patient-related characteristics such as age, sex, history of *H. pylori* infection (either current or past), and dietary habits were not accounted for in analysis due to sample size.

In summary, our results provide a valuable framework for dissecting the complex molecular changes of gastric carcinogenesis, but further work is necessary to clarify the regulatory mechanisms behind post-translational modifications of p65 and p38, and the effects their interactions may have on driving gastric carcinogenesis.

Abbreviations

The following abbreviations are used in this manuscript:

- GC Gastric Cancer.
- IGC Intestinal Gastric Cancer.
- DGC Diffuse Gastric Cancer.
- H.pylori Helicobacter pylori.
- · EGC Early Gastric Cancer.
- CG Chronic Gastritis.
- IM-LGD Intestinal Metaplasia Low-Grade Dysplasia.
- DEPs Differentially Expressed Proteins.
- L Lesional.
- NL Non-lesional

- PGLs Premalignant Gastric Lesions.
- DTT Dithiothreitol.
- CAN-FA Acetonitrile-Formic acid.
- DIA Data-Independent Acquisition.
- FDR False Discovery Rate.

Declarations

Ethics approval and consent to participate: The Navarre Research Ethics Committee approved the study protocol and informed consent on August 27, 2021 (Ref. PI_2021/76).

Consent for publication: Not applicable.

Data availability: Mass-spectrometry data and search results files were deposited in the Proteome Xchange Consortium via the JPOST partner repository (https://repository.jpostdb.org) [1] with the identifier PXD064323 for ProteomeXchange and JPST003828 for jPOST (for reviewers: https://repository.jpostdb.org/preview/29226366968358b4d6d302; Access key: 5398).

Competing interests: Eduardo Albéniz has a consulting agreement with Creo Medical, AGS MedTech, honoraria for lectures, teaching activities or travel grants from Olympus, Boston, Fujifilm, Norgine, Casen Recordati, 3D Matrix. The remaining authors disclose no conflicts.

Funding: This was supported by grants from Instituto de Salud Carlos III (PI21/00333, PI21/01181, PI24/00784 and PI24/00737). Nayra Felípez and Alba Valero have a grant from "Departamento de Universidad, Innovación y Transformación Digital. Gobierno de Navarra", No. 0011-1408-2022-000010 and 0011-1408-2024-000011, respectively. Eduardo Albéniz has a contract for the intensification of research activity in the National Health System, of the 2022 call for Strategic Health Action 2021-2023 (Ref: INT22/00112).

Authorship Contributions:

N.F. conceived and designed the study, performed data curation, validation, and formal analysis, and drafted the original manuscript. J.F.-I., E.S. contributed to study conception and design, conducted formal analysis and validation, curated data, supervised the work, and critically revised the manuscript. S.M. contributed to study conception and design, data acquisition, and supervision, and revised the manuscript. K.A., E.P. performed formal analysis and validation, and revised the manuscript. A.V., J.L., P.D., P.F.-D., E.B., E.A., R.V., M.T.S., A.H., S.P.O., H.N., P.D., A.H., G.H., R.M.S., L.H., C.M.-S., O.P., G.H.-M., M.J.D., S.Z., A.I.D.-M., P.G., D.F., J.S., A.G., A.M.-L., F.E.-A., M.G.A., A.C., F.B., S.C.-B., G.F.-E., M.C. contributed to data acquisition and critically revised the manuscript. L.M., E.A. contributed to the conception and design of the study, acquisition of resources, data curation, supervision, project administration, funding acquisition, and revision of the manuscript. The final manuscript has been approved by all authors.

Acknowledgments:

The authors would like to thank the EpiGASTRIC/EDGAR consortium:

Joan Llach, Sheyla Montori, Anabella Cuestas, Gloria Fernandez-Esparrach, Nayra Felípez, Fermín Estremera-Arévalo, Marta Gómez Alonso, Juan José Vila Costas, Victoria Busto Bea, Juan Carrascosa Gil, Vanesa Jusué Irurita, Alicia Córdoba Iturriagagoitia, Concepción Llanos Chavarri, Irene Amat Villegas, Gregorio Aisa Rivera, Irene Fernández de los Reyes, Gina de Lima Piña, Miguel Ángel Resano, Adriana Yagüe Hernando, Cristina Caballero Martínez, Alfredo López Cousillas, Miriam Cuatrecasas, Pedro Delgado, Javier Tejedor, Elena Arruebo, Silvia Patricia Ortega, Henar Nuñez, Pilar Díez, Diana Zaffalon, Luis Hernández, Gadea Hontoria, Rosa Maria Sáiz, Gonzalo Hijos-Mallada, María José Domper-Arnal, Sara Zarraquiños, Astrid Irene Díez-Martín, Alberto Herreros, Diego de Frutos, Fátima Valentín, José Santiago, Virginia Piñol, Adelina García, Alicia Martín-Lagos, Pablo Florez-Diez, Eva Barreiro, Adolfo Suárez, Raguel Vicente, M Teresa Soria, Cristina Polo, Carmen Yagüe, Alain Huerta, Oiane Rigue Aguinaga, Oliver Patrón, David Tello, Carolina Mangas-Sanjuan, Eva Serrano, Juan Martínez, Rodrigo Jover, Raquel Grajal, Luis Enrique Yip, Patricia Gonçalves, Jenifer Muñoz, Cristina Herrera-Pariente, Laia Bonjoch, Ricard Prat, Sergi Castellví-Bel, Dulce Momblan, Tamara Saurí, Irina Luzko, Elisa Cantú-Germano, Angels Gines, Ignasi Elizalde, Francesc Balaguer, Ángeles Pérez-Aisa, Jennifer Hinojosa, Coral Tejido, Laura Rivas, María Francisco, Manuel Puga, Franco Baiocchi, Cristina Alejandra Sánchez, Alba Pereiros, Joaquin Cubiella, Alejandro Ledo, Ma Victoria Alvarez, Marta Garzón, Juan Manuel Martín, Salvador Sobrino, Ana García-Rodríguez, Inés Gil, Alazne Aguirre, Ainara Maiz, Ines Ariño, María Dolores Pico, Beatriz de Riba, Goretti Hernández, Eduardo Albéniz, Leticia Moreira.

We also thank the Spanish Association of Gastroenterology (AEG) for providing the e-CRF service free of charge.

References

- 1. Moriya, Y. et al. The jpost environment: An integrated proteomics data repository and database. *Nucleic Acids Res.* **47**, D1218–D1224 (2019).
- 2. Bray, F. et al. Global cancer statistics 2022: GLOBOCAN estimates of incidence and mortality worldwide for 36 cancers in 185 countries. *CA Cancer J. Clin.* **74**, 229–263 (2024).
- 3. Mukaisho, K. I., Nakayama, T., Hagiwara, T., Hattori, T. & Sugihara, H. Two distinct etiologies of gastric cardia adenocarcinoma: Interactions among pH, Helicobacter pylori, and bile acids. *Front. Microbiol.*; **6**. (2015).
- 4. Morgan, E. et al. The current and future incidence and mortality of gastric cancer in 185 countries, 2020–40: A population-based modelling study. *EClinicalMedicine* **47**, 101404 (2022).
- 5. Thrift, A. P., Wenker, T. N. & El-Serag, H. B. Global burden of gastric cancer: epidemiological trends, risk factors, screening and prevention. Nat Rev Clin Oncol. Springer Nature; pp. 338–49. (2023).

- 6. Wizenty, J. & Sigal, M. *Helicobacter pylori, microbiota and gastric cancer principles of microorganism-driven carcinogenesis* (Nat Rev Gastroenterol Hepatol. Nature Research, 2025).
- 7. Polk, D. B. & Peek, R. M. Helicobacter pylori: Gastric cancer and beyond. *Nat. Rev. Cancer* pp. 403–414. (2010).
- 8. Correa, P. Human Gastric Carcinogenesis: A Multistep and Multifactorial Process First American Cancer Society Award Lecture on Cancer Epidemiology and Prevention 1 [Internet]. Available from: http://aacrjournals.org/cancerres/article-pdf/52/24/6735/2448984/crs0520246735.pdf
- 9. Comprehensive molecular. characterization of gastric adenocarcinoma. *Nature* **513**, 202–209 (2014).
- 10. Mun, D. G. et al. Proteogenomic Characterization of Human Early-Onset Gastric Cancer. *Cancer Cell.* **35**, 111–124e10 (2019).
- 11. Li, X. et al. Proteomic profiling identifies signatures associated with progression of precancerous gastric lesions and risk of early gastric cancer. *EBioMedicine*;**74**. (2021).
- 12. Shi, W. et al. Multilevel proteomic analyses reveal molecular diversity between diffuse-type and intestinal-type gastric cancer. *Nat. Commun.*;**14**. (2023).
- 13. Tyanova, S. et al. *The Perseus computational platform for comprehensive analysis of (prote)omics data*p. 731–740 (Nat Methods. Nature Publishing Group, 2016).
- 14. Zhou, Y. et al. Metascape provides a biologist-oriented resource for the analysis of systems-level datasets. *Nat. Commun.*;**10**. (2019).
- 15. Krämer, A., Green, J., Pollard, J. & Tugendreich, S. Causal analysis approaches in ingenuity pathway analysis. *Bioinformatics* **30**, 523–530 (2014).
- 16. Song, B. et al. Biomarker identification of chronic atrophic gastritis and its potential drug analysis. *Front. Gastroenterol.*; **1**. (2022).
- 17. Juan Carlos Oliveros & Oliveros, J. C. Venny. An interactive tool for comparing lists with Venn's diagrams. (2007–2015). https://bioinfogp.cnb.csic.es/tools/venny/index.html
- 18. Ellis, E. M., Judaht, D. J., Nealt, G. E. & Hayes, J. D. An ethoxyquin-inducible aldehyde reductase from rat liver that metabolizes aflatoxin B1 defines a subfamily of aldo-keto reductases (chemprotection/liver cancer/antioiddant). Proc. Natl. Acad. Sci. USA. (1993).
- 19. Krämer, A., Green, J., Pollard, J. & Tugendreich, S. Causal analysis approaches in ingenuity pathway analysis. *Bioinformatics* **30**, 523–530 (2014).
- 20. Li, B. et al. CREB1 contributes colorectal cancer cell plasticity by regulating lncRNA CCAT1 and NF-κB pathways. *Sci. China Life Sci.* **65**, 1481–1497 (2022).
- 21. Linnskog, R., Jönsson, G., Axelsson, L., Prasad, C. P. & Andersson, T. Interleukin-6 drives melanoma cell motility through p38α-MAPK-dependent up-regulation of WNT5A expression. *Mol. Oncol.* **8**, 1365–1378 (2014).
- 22. Jiang, H. & Li, H. Prognostic values of tumoral MMP2 and MMP9 overexpression in breast cancer: a systematic review and meta-analysis. *BMC Cancer*;**21**. (2021).

- 23. Taniguchi, K. & Karin, M. NF-kB, inflammation, immunity and cancer: Coming of age. *Nat. Rev. Immunol. Nat. Publishing Group.*; pp. 309–324. (2018).
- 24. Wang, D. J., Ratnam, N. M., Byrd, J. C. & Guttridge, D. C. NF-κB functions in tumor initiation by suppressing the surveillance of both innate and adaptive immune cells. *Cell. Rep.* **9**, 90–103 (2014).
- 25. Li, Y. et al. *Inhibition of NF-κB signaling unveils novel strategies to overcome drug resistance in cancers* (Drug Resistance Updates. Churchill Livingstone, 2024).
- 26. Luo, J. L., Kamata, H. & Karin, M. IKK/NF-κB signaling: Balancing life and death A new approach to cancer therapy. *J. Clin. Invest.* pp. 2625–2632. (2005).
- 27. Mirzaei, S. et al. NF-κB as a regulator of cancer metastasis and therapy response: A focus on epithelial–mesenchymal transition. J Cell Physiol. John Wiley and Sons Inc; pp. 2770–95. (2022).
- 28. Verzella, D. et al. Life, death, and autophagy in cancer: NF-κB turns up everywhere. Cell Death Dis. Springer Nature; (2020).
- 29. Christian, F., Smith, E. L. & Carmody, R. J. *The regulation of NF-κB Subunits by Phosphorylation* (Cells. MDPI, 2016).
- 30. Sun, X. et al. *Post-translational modifications of p65: state of the art* (Front Cell Dev Biol. Frontiers Media SA, 2024).
- 31. Lewander, A. et al. NF-κB p65 phosphorylated at serine-536 is an independent prognostic factor in Swedish colorectal cancer patients. *Int. J. Colorectal Dis.* **27**, 447–452 (2012).
- 32. Xu, X. et al. Phosphorylation of NF-κBp65 drives inflammation-mediated hepatocellular carcinogenesis and is a novel therapeutic target. *J. Experimental Clin. Cancer Res.*; **40**. (2021).
- 33. Pradère, J. P. et al. Negative regulation of NF-κB p65 activity by serine 536 phosphorylation. *Sci. Signal.*; **9**. (2016).
- 34. Aoki, T. et al. Phosphorylation of Serine 536 of p65(RelA) Downregulates Inflammatory Responses. Inflammation.; (2024).
- 35. Mantovani, A., Allavena, P., Sica, A. & Balkwill, F. Cancer-related inflammation. *Nature* pp. 436–444. (2008).
- 36. Yang, M. & Huang, C. Z. Mitogen-activated protein kinase signaling pathway and invasion and metastasis of gastric cancer. *World J. Gastroenterol.* **21**, 11673–11679 (2015).
- 37. Phan, T., Zhang, X. H., Rosen, S. & Melstrom, L. G. *P38 kinase in gastrointestinal cancers. Cancer Gene Ther*p. 1181–1189 (Springer Nature, 2023).
- 38. Yin, N. et al. P38γ MAPK is required for inflammation-associated colon tumorigenesis. *Oncogene* **35**, 1039–1048 (2016).
- 39. Gupta, J. et al. Dual Function of p38α MAPK in Colon Cancer: Suppression of Colitis-Associated Tumor Initiation but Requirement for Cancer Cell Survival. *Cancer Cell.* **25**, 484–500 (2014).
- 40. Zhang, W., Liu, H. T. & Tu, H. MAPK signal pathways in the regulation of cell proliferation in mammalian cells [Internet]. Cell Res. (2002). Available from: http://www.cell-research.com

- 41. Zarubin, T. & Han, J. Activation and signaling of the p38 MAP kinase pathway [Internet]. Cell Res. Available from: www.cell-research.com| (2005).
- 42. Hardwick, J. C., Van Den Brink, G. R., O€erhaus, G. J., Van Jh, S. & Peppelenbosch, M. P. NF-kappaB, p38 MAPK and JNK are highly expressed and active in the stroma of human colonic adenomatous polyps [Internet]. Available from: www.nature.com/onc
- 43. Wang, G. et al. Her2 promotes early dissemination of breast cancer by inhibiting the p38 pathway through the downregulation of MAP3K4. *Cell. Communication Signal.*; **22**. (2024).
- 44. MacNeil, A. J. et al. MAPK kinase 3 Is a tumor suppressor with reduced copy number in breast cancer. *Cancer Res.* **74**, 162–172 (2014).
- 45. Canovas, B. & Nebreda, A. R. Diversity and versatility of p38 kinase signalling in health and disease. *Nat. Rev. Mol. Cell. Biol. Nat. Res.*; pp. 346–366. (2021).
- 46. MAPKK-Independent Activation. of p38 Mediated by TAB1-Dependent Autophosphorylation of p38.
- 47. Salvador, J. M. et al. Alternative p38 activation pathway mediated by T cell receptor-proximal tyrosine kinases. *Nat. Immunol.* **6**, 390–395 (2005).

Figures

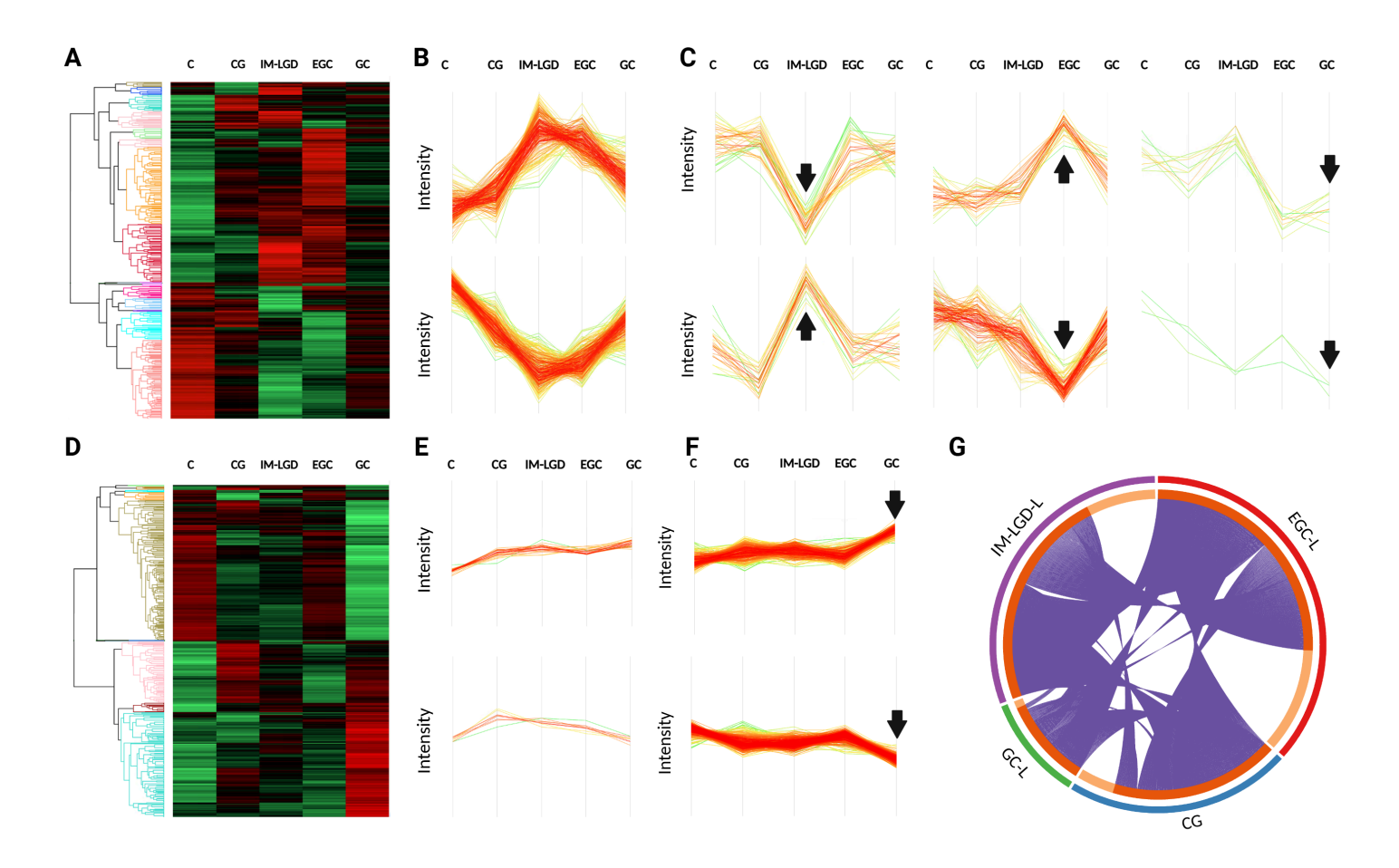


Figure 1

Proteomic variations in digestive tissue at different stages of gastric carcinogenesis. **A**. Heatmap showing the proteome of biopsies from L gastric tissue across groups C, G, IM-LGD, EGC, and GC. **B**. Protein clusters associated with disease progression. **C**. Protein clusters peaking at various stages. D. Heatmap showing the proteome of biopsies from NL gastric tissue across groups C, G, IM-LGD, EGC, and GC. **E**. Protein clusters associated with disease progression. **F**. Protein clusters peaking in the GC stage (non-tumoral tissue). **G**. Circos plot representing the deregulated proteome in stomach tissue shared between lesions. Inside, dark orange indicates proteins shared by multiple lists, while light orange indicates proteins unique to a dataset. Purple lines connect proteins shared across biological conditions. (CG = chronic gastritis, IM-LGD = intestinal metaplasia-low grade dysplasia, EGC = early gastric cancer, and GC = gastric cancer, NL = non-lesional, L = lesional).

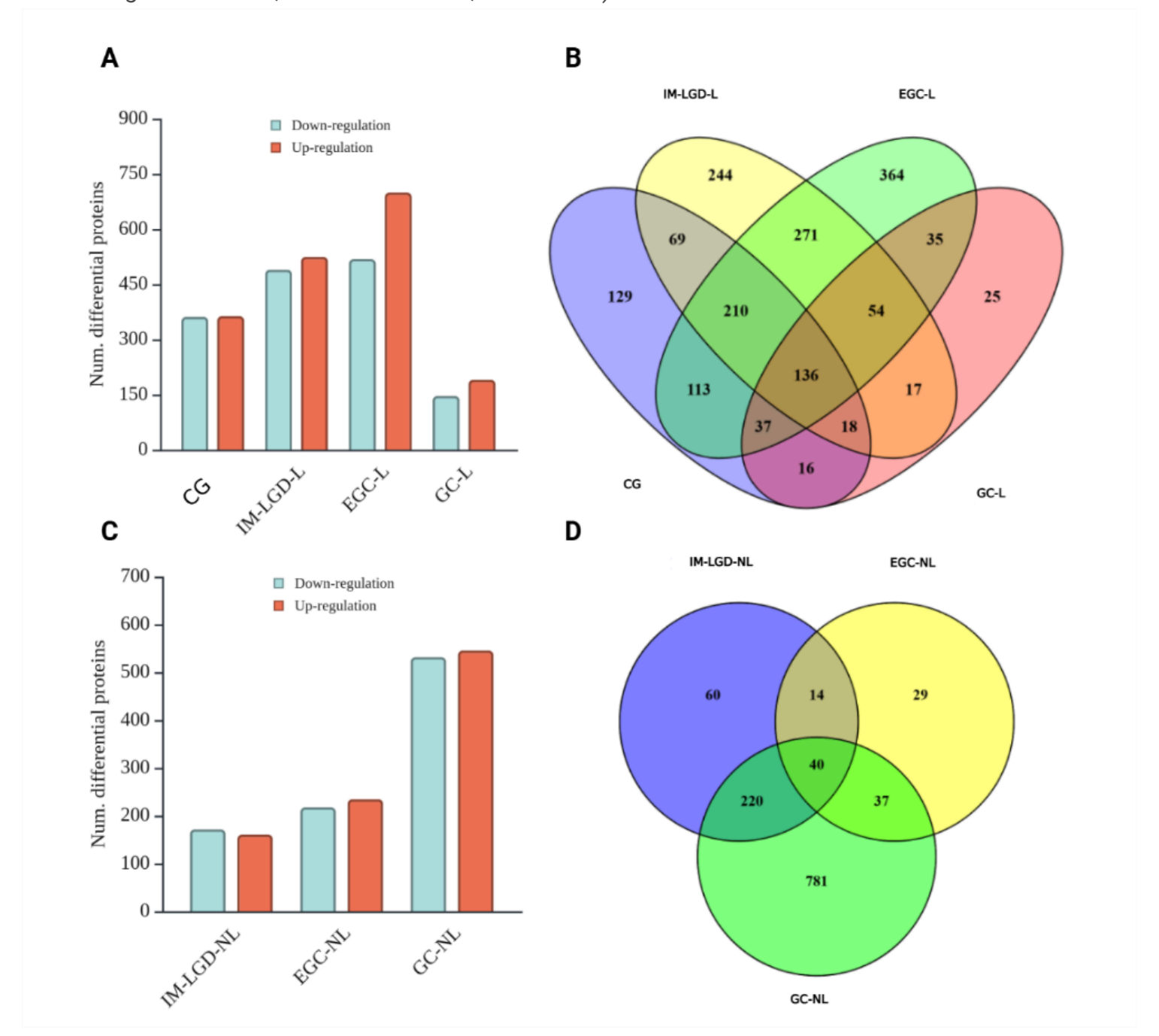


Figure 2

Differentially expressed proteins in the stomach across CG, IM-LGD, EGC, and GC. **A**. Differential gastric proteome distribution across L stages. **B**. Venn diagram of standard and unique differential protein between lesional stages. **C**. Differential stomach proteome distribution across non-lesional stages. **D**. Venn diagram of standard and unique differential protein between non-lesional stages. (CG = chronic gastritis, IM-LGD = intestinal metaplasia-low grade dysplasia, EGC = early gastric cancer, and GC = gastric cancer, NL = non-lesional, L = lesional). Barplots were made using Biorender.com and diagrams with online tool [17].

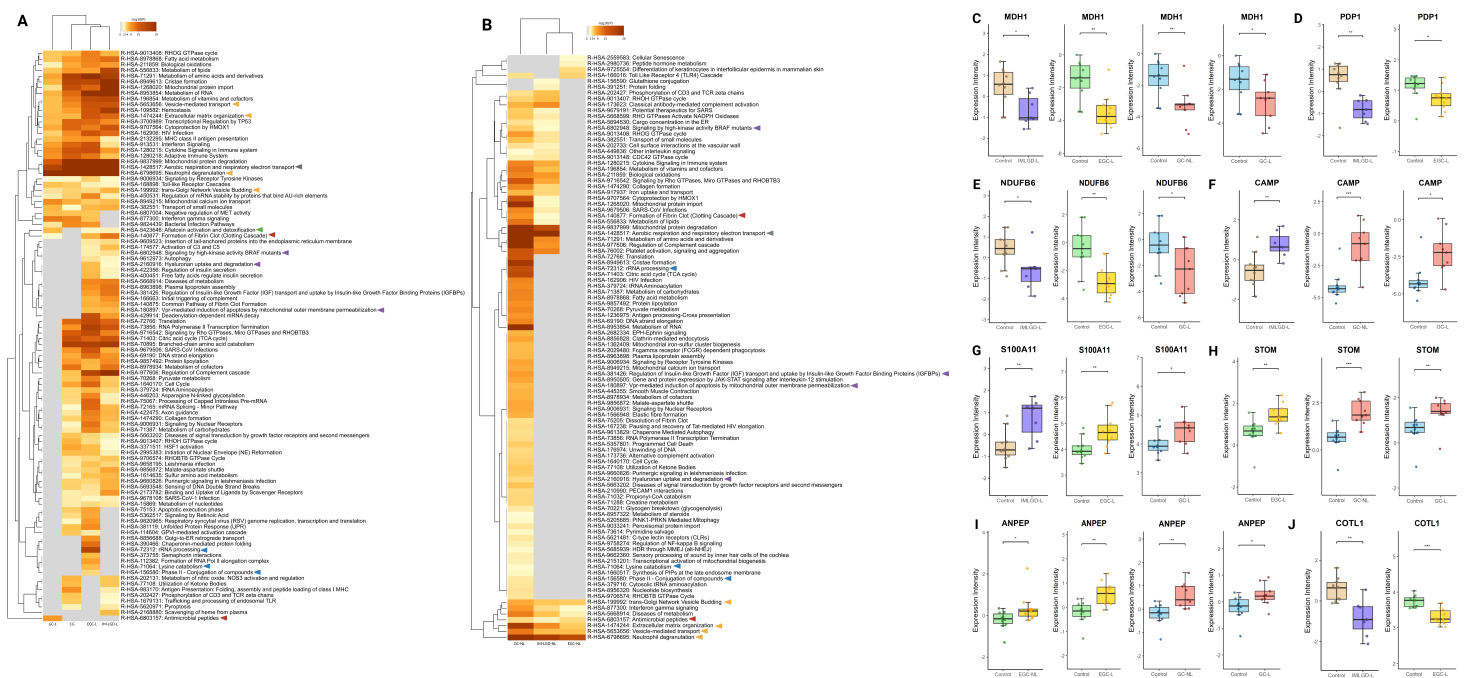


Figure 3

Pathway enrichment and protein expression changes in gastric tissue. **A, B**. Heatmaps illustrating commonly enriched pathways in L and NL gastric tissue across different disease stages using Reactome database through Metascape tool. Yellow arrows indicate biological processes commonly altered in L and NL tissues in all cohorts. The green arrow indicates a biological process only presented in lesions. Blue arrows indicate biological processes commonly altered in EGC-L and GC-NL. **C**. Boxplots of MDH1 protein expression changes in IM-LGD-L, EGC-L, GC-NL, and GC-L. **D**. Boxplots of PDP1 protein expression changes in IM-LGD-L and EGC-L. **E**. Boxplots of NDUFB6 protein expression changes in IM-LGD-L, GC-NL, and GC-L. **G**. Boxplots of S100A11 protein expression changes in IM-LGD-L, EGC-L, and GC-L. **H**. Boxplots of STOM protein expression changes in EGC-L, GC-NL and GC-L. I. Boxplots of ANPEP protein expression changes in EGC-NL, EGC-L, GC-NL and GC-L. J. Boxplots of COTL1 protein expression changes in IM-LGD-L and EGC-L. Boxplots show the distribution of protein expression intensity in each group vs.control group. The box represents the interquartile range (IQR), the line within the box is the median, and the whiskers extend to 1.5 times the IQR. Individual points represent the expression in each sample. Error bars represent the IQR. Significance labels indicate the statistical significance of the difference between

groups: *p < 0.05, **p < 0.01, and ***p < 0.001. (CG = chronic gastritis, IM-LGD = intestinal metaplasia-low grade dysplasia, EGC = early gastric cancer, and GC = gastric cancer, NL = non-lesional, L = lesional).

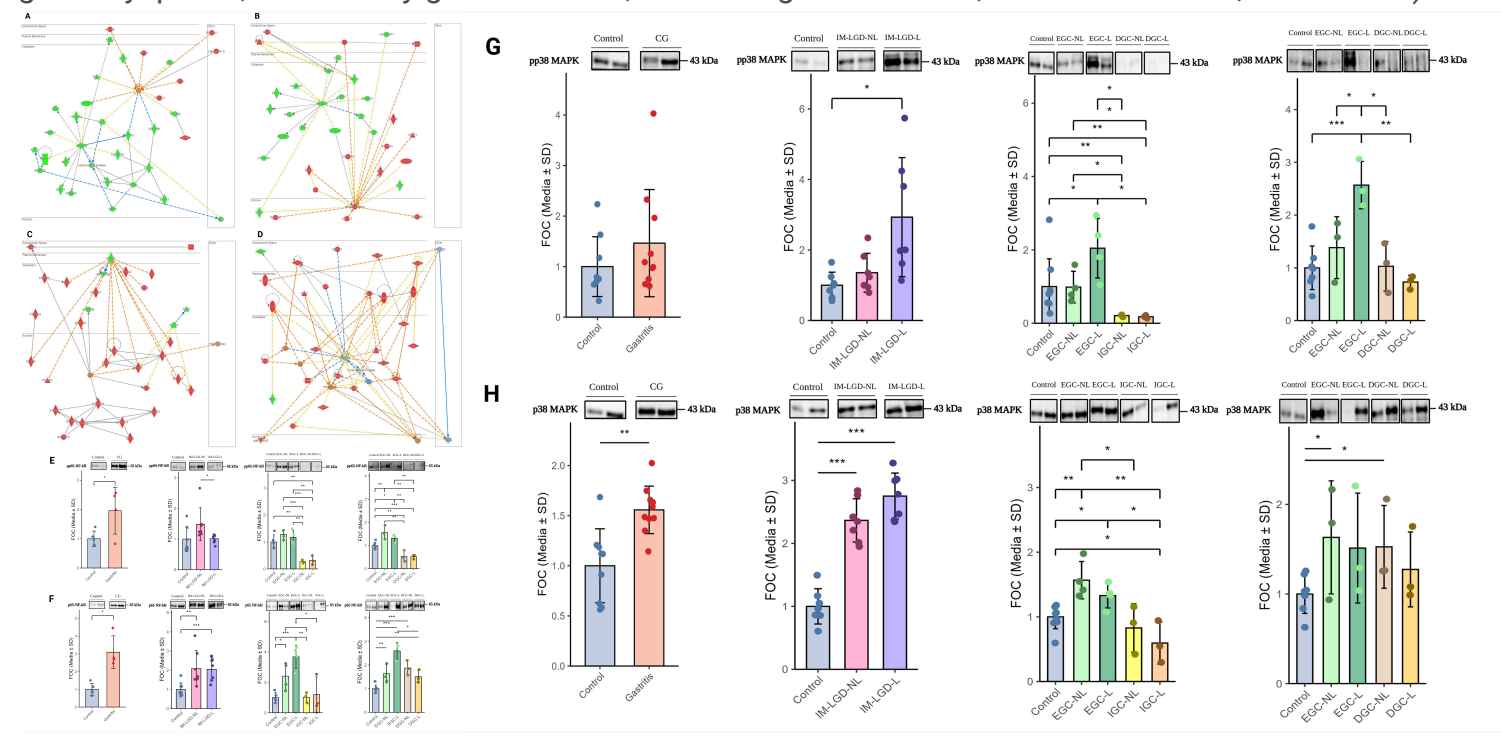


Figure 4

Protein interaction network maps generate by IPA software and western blot expression levels of p65-NF-kB and p38 MAPK, in CG, IM-LGD, EGC, and GC. Functional networks associated with CG (A), IM-LGD-L (B), EGC-L (C), and GC-L (D). Green and red indicate down and up-regulated proteins, respectively. Orange and blue indications are activation or inhibitory mechanisms proposed by the IPA algorithm. Protein expression levels of pp65-NF-kB (E) and p65-NF-kB (F) across Control, IM-LGD-NL, IM-LGD-L, EGC-NL, EGC-NL, IGC-NL, IGC-L, DGC-NL, and DGC-L. Protein expression levels of pp38-MAPK (G) and p38-MAPK (H) across Control, IM-LGD-NL, IM-LGD-L, EGC-NL, EGC-L, IGC-NL, IGC-L, DGC-NL, and DGC-L. Western blotting was performed, and representative images are shown. Equal gel loading was confirmed using stain-free digitalization. The panels display histograms of band densities. The quantification of Fig.4E-H were analysed by ImageLab. The blots were cropped from different gels. Uncropped blots are available in Supplementary 5. Data are presented as mean ± SD. *p < 0.05; **p < 0.01, ***p < 0.001 vs. control group and between groups (FOC: fold of change, CG = chronic gastritis, IM-LGD = intestinal metaplasia-low grade dysplasia, EGC = early gastric cancer, GC = gastric cancer, IGC = intestinal gastric cancer, DGC = diffuse gastric cancer, NL = non-lesional, L = lesional).

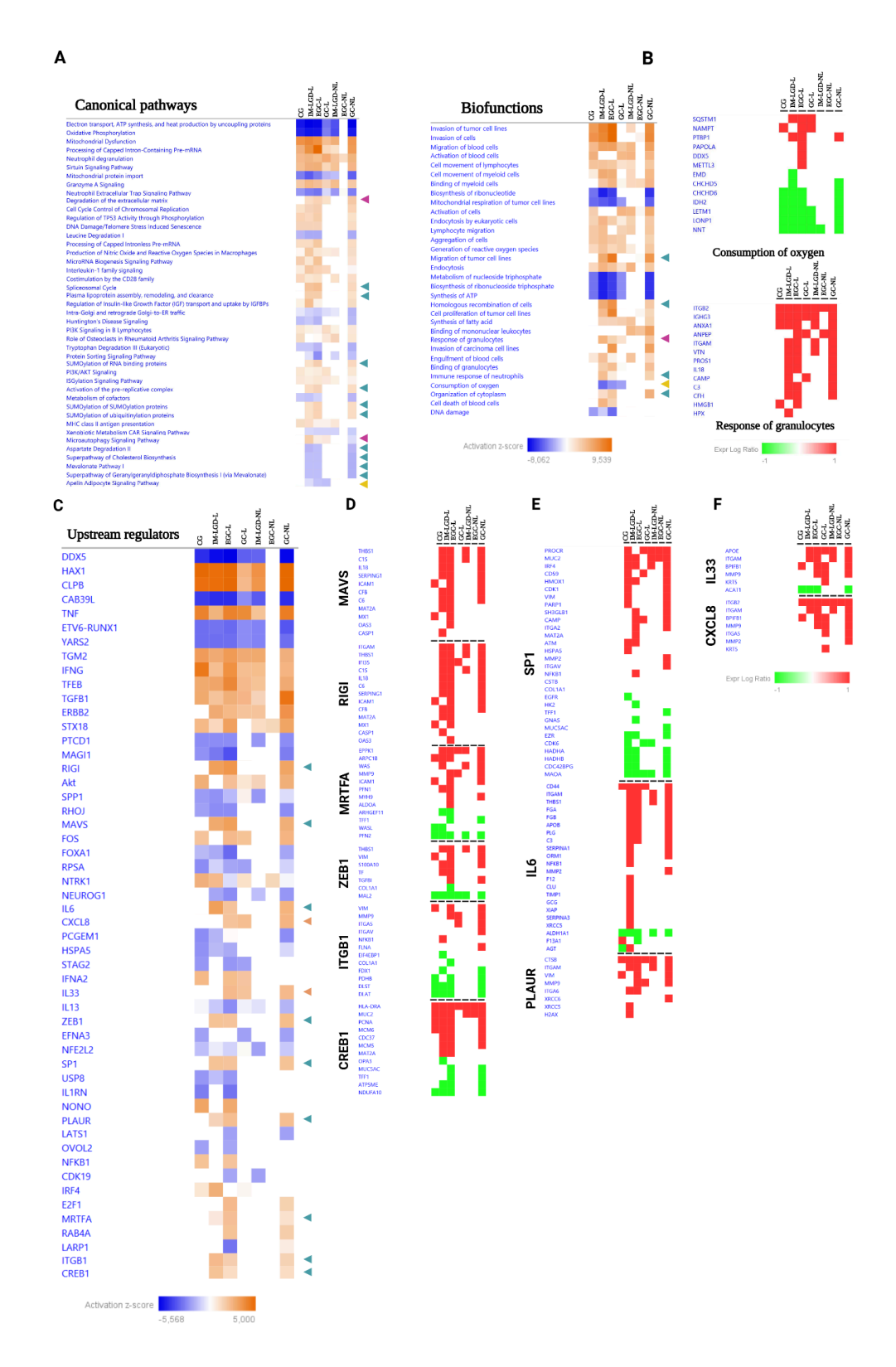


Figure 5

Predictive activation profile of pathways, biofunctions and upstream regulators in gastric carcinogenesis. Based on proteomic data sets for each stage (lesion and non-lesion), Systems Biology analysis was performed through the Ingenuity Pathway Analysis software [19]. Activation prediction of significantly altered pathways and biofunctions (A, B) and upstream regulators (C-F). The activation z-score is calculated as previously described [19]. It makes predictions about potential regulators using

information about the direction of protein regulation and comparing it with a model that assigns random regulation directions. Blue and orange squares indicate inhibition and activation directionality, respectively. Blue triangles refer to processes/molecules with an activation score exclusively associated with IM-LGD-L, EGC-L, and GC-NL. Orange triangles indicate molecules with an activation profile associated with EGC-L, GC-L, and GC-NL. Red triangles refer to processes with an activation score exclusively associated with IM-LGD-L, EGC-L, and GC-NL. Yellow triangles refer to processes with an activation score exclusively associated with IM-LGD-L, EGC-L, and GC-L. Red: up-regulation; green: down-regulation (CG = chronic gastritis, IM-LGD= intestinal metaplasia-low grade dysplasia, EGC = early gastric cancer, GC = gastric cancer, NL = non-lesional, L = lesional).

Supplementary Files

This is a list of supplementary files associated with this preprint. Click to download.

- floatimage1.png
- SupplementaryMaterial1.xlsx
- SupplementaryMaterial2.pdf
- SupplementaryMaterial3.xlsx
- SupplementaryMaterial4.xlsx
- SupplementaryMaterial5.pdf